SHocks: structure, AcceleRation, dissiPation

Work Package 3
Particle energization and dissipation processes at shocks

Deliverable D3.2
Technical report on the effects of rippling and non-stationarity on the ion distributions in the shock front

Andrew P. Dimmock[1], Daniel Graham[1], Ahmad Lalti[1], Yuri Khotyaintsev[1], Ajay Lotekar[1†], Michael Gedalin[2]

[1] Swedish Institute of Space Physics, Uppsala, Sweden, [2] Ben-Gurion University, Israel
[†] Deceased

13/12/2022

This project has received funding from the European Union's Horizon 2020 research and innovation programme under grant agreement No 101004131

Document Change Record

Issue	Date	Author	Details
1	13/12/2022	A.P. Dimmock	First draft
2	16/12/2022	A.P. Dimmock	Revised after co-authors comments

Table of Contents

1 Summary

This technical report serves as an overview of the investigation of phase space holes (PSHs), which are a manifestation of shock ripples in the ion velocity distribution function at the Earth's bow shock. The study automatically identifies shocks with PSHs based on the reduced ion distribution, which is applied to the bow shock database by Lalti et al. [2022] that contains 2797 shocks. The main results are that PSHs are expected 66% of the time, increase in probability with Alfvén Mach number, and the likelihood of observing them with spacecraft can be dictated by the shock speed.

2 Introduction

Plasma shocks are ubiquitous in the Universe, appearing around planets [Russell, 1985], the outer periphery of the heliosphere [Jokipii, 2013], and supernova remnants [Bell, 2013, Helder et al., 2012]. For heliospheric plasma shocks, particle collisions are so rare that their effects on the shock can be neglected, hence such shocks are named collisionless. They efficiently convert kinetic energy into thermal energy via the interactions between particles and electromagnetic fields. Yet, the structure of collisionless shocks can be highly complex, with internal structures that span multiple scales, which are delicately coupled to shock parameters. Thus, connecting the magnetic structure of the shock front to energy dissipation processes has been the subject of extensive research for decades and still many open questions remain.

Collisionless shocks are characterized by parameters such as the Alfvén Mach number (M_A), plasma beta (β) and geometry (θ_{Bn}), which is the angle between the upstream magnetic field and the shock normal direction ($\hat{\mathbf{n}}$). In this context, quasi-parallel shocks have $\theta_{Bn} < 45°$ and quasi-perpendicular shocks have $\theta_{Bn} > 45°$. The shock geometry plays a pivotal role in how plasma is processed and this dictates both the structure of the shock itself and also the plasma dynamics upstream and downstream. In this report, we consider only quasi-perpendicular shocks.

For quasi-perpendicular shocks, a fraction of the incident ions are reflected and gyrates immediately upstream, gaining energy from the solar wind convective electric field before passing downstream. The typical characteristics of a quasi-perpendicular shock are the foot, ramp, and overshoot regions. In addition, the reflected ions cause a high anisotropy in the velocity distribution, which can subsequently drive waves and instabilities such as whistler waves. At supercritical shocks, which, is typically the case at the Earth's bow shock, these processes (i.e. ion reflection, whistler waves) play a fundamental role in energy dissipation. However, if M_A gets sufficiently large, additional processes are required. In these high M_A regimes, the shock can evolve to be nonstationary and eventually undergo reformation, which is a cyclic large-scale magnetic restructuring of the shock front [Russell et al., 1982, Lembege and Dawson, 1987, 1989, Winterhalter and Kivelson, 1988, Krasnoselskikh et al., 2002, Dimmock et al., 2019].

Another state of shock nonstationarity is shock rippling, which is commonly described as a wave-like structure propagating along the shock surface and has a direction that is tangential to the shock normal direction [Johlander et al., 2016].

When a spacecraft observes shock ripples, the characteristic response is deviations in shock parameters such as magnetic field direction and density [Burgess and Scholer, 2007]. Moullard et al. [2006] presented such observations made by the Cluster spacecraft, which were attributed to ripples. Afterwards, Johlander et al. [2016] reported observation of surface ripples at the quasi-perpendicular shock using MMS observations. In that study, ripples were confirmed using multi-spacecraft observations and high-cadence plasma measurements. Interestingly, the ripple period was comparable to the local ion gyroperiod. Nevertheless, studies of shock ripples are not restricted to experimental studies. Using simulations, Winske and Quest [1988] proposed that ripples can be caused by the Alfvén ion cyclotron (AIC) instability. Using test particle simulations, Yang et al. [2012] showed that shock ripples can influence the characteristics of ion reflection at the shock front.

So far, the majority of shock ripple investigations have been founded on simulations and/or detailed case studies such as that by Johlander et al. [2016]. For this reason, we conduct a statistical study of shock ripples that links their occurrence and properties to shock parameters and upstream conditions. To do this, we devised an automated method to identify rippled shocks, which was then applied to the shock database compiled by Lalti et al. [2022] that contains 2797 bow shock crossings by the Magnetospheric Multiscale Mission (MMS).

The report is organised as follows. We first introduce the data and methodology, which describes how rippled shocks are identified and characterized. Next, the major results are presented before discussing the results and drawing the central conclusions.

3 Data sets

This study employs Earth bow shock crossings made by MMS during burst mode up to December 2020. The data used are magnetic field at a 128 Hz provided by the fluxgate magnetometers (FGM) [Russell et al., 2016] and 3D distribution at 150 ms provided by the fast plasma investigators dual ion spectrometer (FPI-DIS) [Pollock et al., 2016].

The shock crossings utilised in this study are taken from the MMS shock database compiled by Lalti et al. [2022]. This database utilizes the results of Olshevsky et al. [2021], which employs a neural network algorithm to classify MMS data according to the attributes of the 3D ion distribution function. The MMS data is classified according to the solar wind, magnetosheath, foreshock, and magnetosphere regions. Bow shock crossings are determined from the classification shift from the foreshock-magnetosheath, solar wind-magnetosheath, and vice-versa. For each shock, the database provides key shock parameters such as M_A, $\hat{\mathbf{n}}$, and θ_{Bn}, as well as upstream solar wind properties such as the magnetic field vector B_u and solar wind bulk velocity V_u. For all the shocks, $\hat{\mathbf{n}}$ is calculated from the Farris bow shock model [Farris et al., 1991], and upstream parameters are retrieved from the OMNI service [King and Papitashvili, 2005]. We direct readers to Lalti et al. [2022] for a more detailed description of the database.

4 Methodology

For this study, we extract quasi-perpendicular shocks from the database according to $\theta_{Bn} > 45°$. We also require burst mode data, observations are available to calculate all parameters, and the shock transition shows clear solar wind/magnetosheath regions. This yields 516 viable shock crossings for the study. Figure 1 shows the statistical distribution of M_A and θ_{Bn} for the shocks used in this study. According to Figure 1a the majority of shocks have $M_A \sim 5 - 10$, however, there

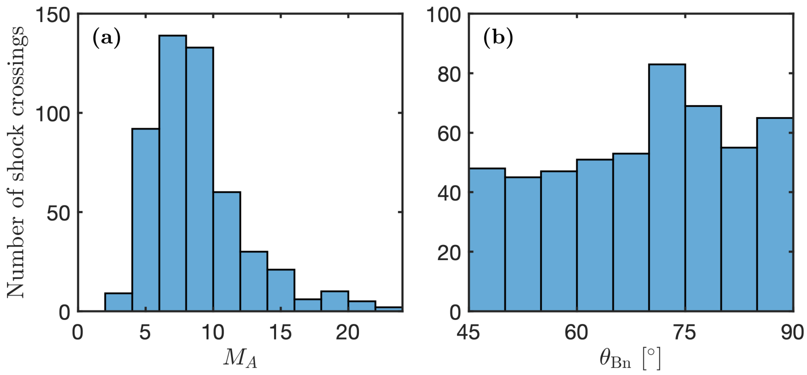

Figure 1: Statistical distribution of M_A and θ_{Bn} for the shocks used in the study.

is a tail with M_A exceeding 20. The shock geometry is quite evenly distributed between $45° - 90°$, with slightly more shocks between $75° - 90°$. However, we do not anticipate this to influence the later statistical results.

For each shock, it is required to decide if it is rippled or not, and how many ripples are observed by the spacecraft. To do this, we exploit the reported observations by Johlander et al. [2016] that revealed shock ripples were accompanied by modulations in the 1D reduced (along $\hat{\mathbf{n}}$) ion distribution. As a spacecraft is located within the shock front, ripples will cause it to periodically transition between the foot and downstream as it transits each ripple. Thus, numerous reflected ion populations will be observed together with their matching reflection points. In practice, this manifests as holes in phase space, the hole referring to the drop in phase space that is radially bounded by the reflected ions and their reflection point, as shown in Figure 2. From here on we refer to these as phase space holes (PSHs), which are used to classify shocks as rippled.

An automated procedure was devised to identify PSHs in each shock, as well as the number of PSHs observed. We adopted a contour approach since PSHs can be deemed local 3D minima in phase space. The process is as follows:

1. Reduce the 3D velocity distribution along $\hat{\mathbf{n}}$.
2. Apply a Gaussian filter to remove the impact from small-scale (smaller than the hole) variations and prevent over-identification.
3. Manually selects the crossing time, which is selected from early signs of reflected ions to the last reflection point.
4. Map contours to the filtered reduced distribution.
5. Remove open contours and any max

6. Remove contours with nonphysical dimensions, e.g. much longer than the shock itself.

7. Keep contours with circular/elliptical shapes based on if the geometrical center lies within the contour bounds.

8. Remove outliers based on contours that have less than two points inside.

9. PSHs are identified from the largest contour that bounds at least two remaining ones.

The MATLAB routine for this is named irf_shock_psh_id and is publicly available in IRFU-MATLAB.

Figure 2 shows an example of the PSH identification for three separate shocks of varying PSH numbers. Each sub-figure shows the date, parameters, and number of PSHs for each of the shock crossings. The shock on 2015-10-17 exhibits one

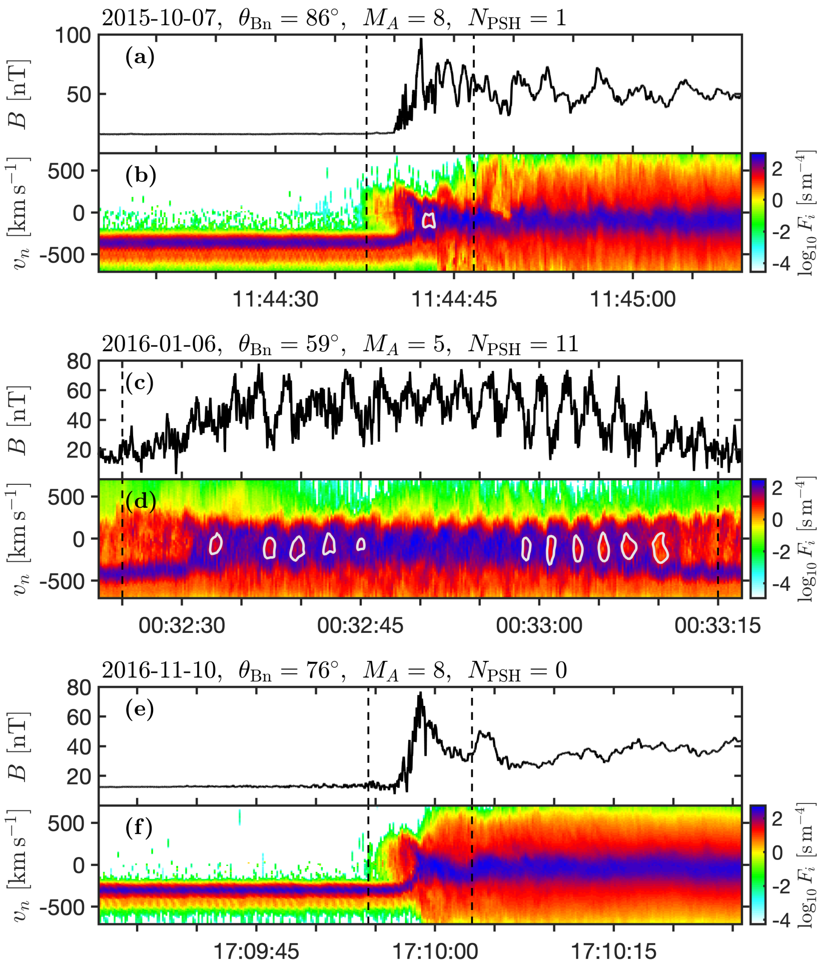

Figure 2: Identification of PSHs for three different shocks that exhibit varying numbers of PSHs.

PSH as demonstrated by the white boundary, whereas the shock on 2016-01-06 was a highly rippled shock with 11 PSHs. The last example on 2016-11-10 did not contain any PSHs. From limited event such as these, it is far from obvious how shock parameters are connected to the number of PSHs and also the properties of the PSHs themselves. Thus, this figure exemplifies the motivation of this study to take a statistical approach to this problem. In the next section, we will investigate the relationship between PSHs and fundamental shock parameters.

5 Results & Discussion

Figure 3 investigates the probability of PSHs for the shocks included in the database. Here, $P(N_{PSH})$ is defined as the probability of observing at least 1 PSH. Panel (a) reveals the occurrence of the number of PSHs (N_{PSH}) for the

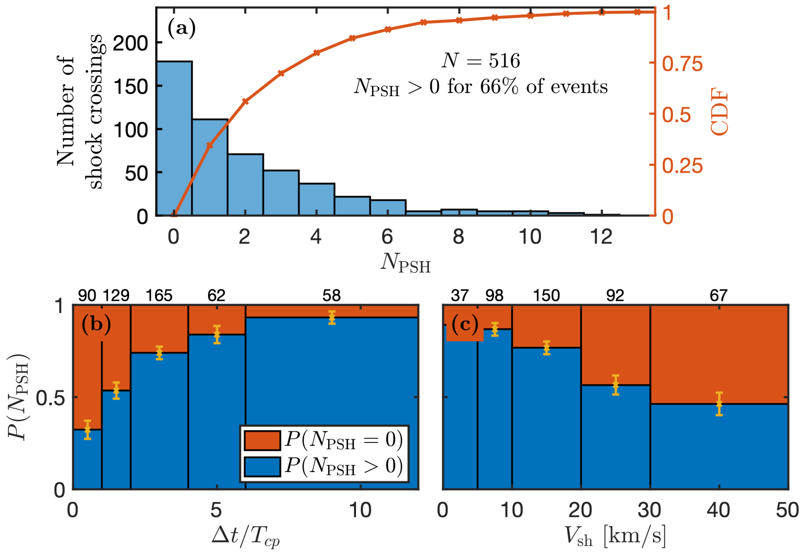

Figure 3: Cumulative distribution of PSHs (a), $P(N_{PSH})$ for the normalised shock crossing time, and various shock speeds.

shocks included in this study. An obvious result is that shocks with PSHs>6 are quite rare, indicating that the shock that was shown in Figure 2 with 11 PSHs is not a typical event. Yet, shocks with at least 1 PSH are relatively common, occurring 66% of the time. Also, we did not see a clear optimal number of PSHs for the 516 shock crossings that were analyzed. We can deduce that PSHs are common, but only in small numbers.

The above result can be more readily understood by panels (b & c) in Figure 3 that show $P(N_{PSH})$ for the normalized shock crossing time (to the ion gyroperiod), and the shock speed. Panel (b) shows a proportional association, that the longer normalized shock crossing times offer higher probabilities of PSH detection. This is reinforced by panel (c) since slower shocks provide a higher probability. In other words, slower shocks provide more time for the spacecraft to observe PSHs. This demonstrates a key result in that the PSHs observed at Earth's bow shock by spacecraft are intrinsically connected to the physical scale lengths of the shock and the shock speed itself.

Figure 4 below shows $P(N_{PSH})$ for various shock parameters. In panel (c), M_{nw} is the nonlinear critical whistler Mach number [Krasnoselskikh et al., 2002, Dimmock et al., 2019] and tells when we expect a shock to reform according to

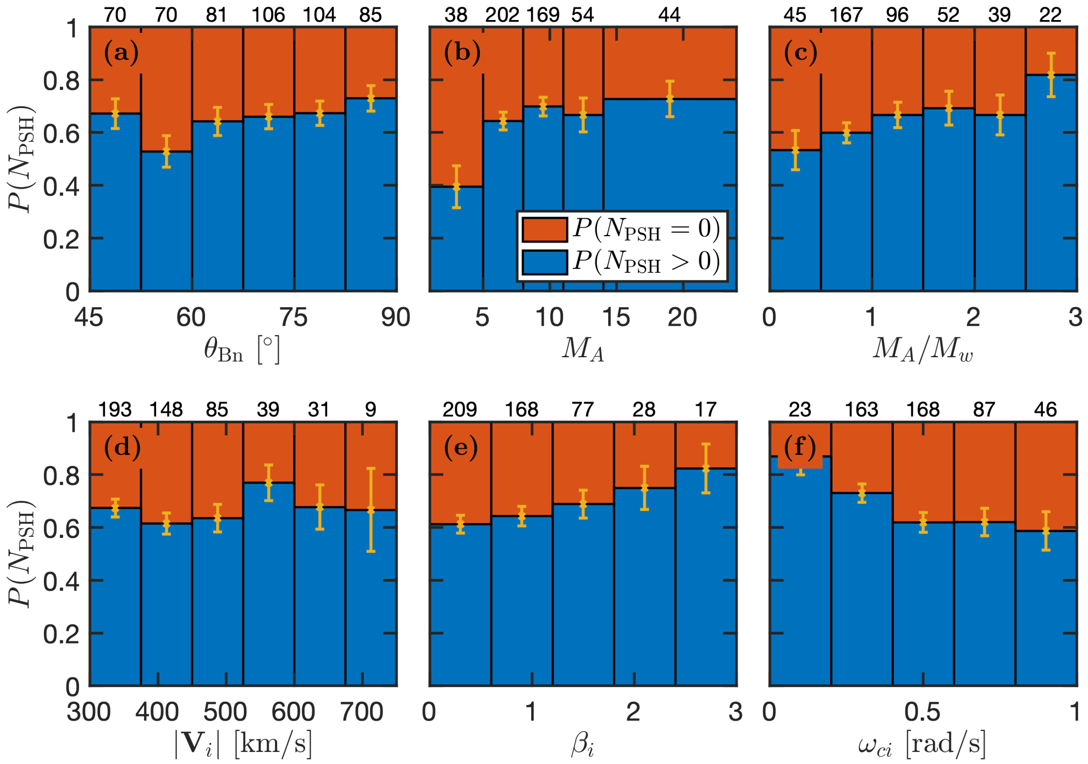

Figure 4: The panels (a-f) show $P(N_{PSH})$ for θ_{bn}, M_A, M_A/M_w, $|\mathbf{V_i}|$, β_i, and ω_{ci}.

a gradient catastrophe mechanism. Some parameters do not show clear dependencies such as θ_{bn}, and $|\mathbf{V_i}|$. Interestingly, panel (b) proposes that at higher M_A, $P(N_{PSH})$ increases from around 0.4 to 0.7. This implies that shock rippling is inherently connected to M_A. Nevertheless, we also see a trend in panel (c), which could indicate that PSHs may be related to M_{nw}. For periodically reforming shocks, we could expect to see PSHs as the reformation process has been suggested to occur on ion gyroscales, comparable to shock ripples. Such a reformation would manifest as modulations in the reduced ion distributions. Thus, numerous mechanisms may contribute to the formation of PSHs at the shock front. Disentangling these mechanisms is not the focus of this study and requires scrutinizing individual shock crossings. One method to separate such events would be to examine the local shock normal since ripples are expected to deviate from this. On the other hand, reforming shocks would be expected to contain similar shock normal directions if the upstream field remained stable.

Figure 5 shows the dimensional of the PSHs that were identified. Panel (a) considers the velocity spread as a function of the upstream solar wind speed whereas panel (b) the temporal width against the ion gyroperiod. Panel (a) suggests that solar wind speed plays a considerable role in the velocity width of the observed PSHs. This implies that faster solar wind speeds will cause a stronger reflected ion population; since PSHs are measured between the incident and reflected ion populations, the vertical dimension will increase. There is some indication of a dependency on the ion gyroradius, especially since the spread increases for larger τ_{ci}. Still, this dependency is unclear and deserves additional investigation.

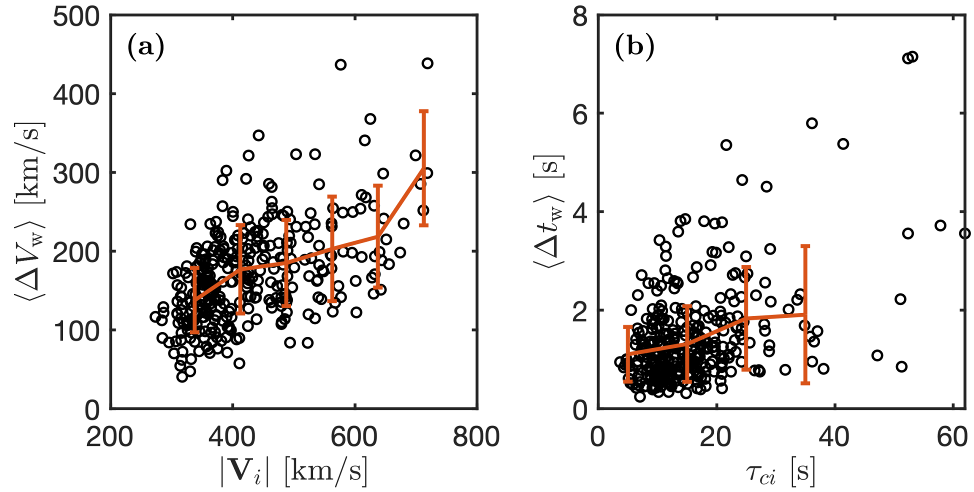

Figure 5: The velocity and temporal width of PSHs plotted against the upstream ion speed (a) and ion gyroradius (b), respectively.

6 Conclusions

We have conducted the first statistical study of PSHs at quasi-perpendicular shocks and their association to shock parameters. From this study we can draw the following conclusions:

1. PSHs are common and occurred for 66% of all the examined shocks, however, the true occurrence is likely higher.
2. The number of PSHs is generally low (<6) and highly rippled shocks (10 or more) are rare.
3. The shock speed and normalised scale plays a fundamental role in the ability of a spacecraft to observe PSHs since the number of PSHs was significantly larger for slower and longer shock crossings.
4. The probability of observing at least one PSH grows with the Alfvén Mach number.
5. There are some indications that shock reformation could play a role in generating PSH features in the reduced ion distributions. Regardless, this requires a more exhaustive investigation.

7 References

A. R Bell. Cosmic ray acceleration. *Astroparticle Physics*, 43:56–70, 2013.

D. Burgess and M. Scholer. Shock front instability associated with reflected ions at the perpendicular shock. *Physics of Plasmas*, 14(1):012108, 2007. doi: 10.1063/1.2435317.

A. P. Dimmock, C. T. Russell, R. Z. Sagdeev, V. Krasnoselskikh, S. N. Walker, C. Carr, I. Dandouras, C. P. Escoubet, N. Ganushkina, M. Gedalin, Yu. V. Khotyaintsev, H. Aryan, T. I. Pulkkinen, and M. A. Balikhin. Direct evidence of nonstationary collisionless shocks in space plasmas. *Science Advances*, 5(2): eaau9926, February 2019. doi: 10.1126/sciadv.aau9926.

M. H Farris, SM Petrinec, and C. T Russell. The thickness of the magnetosheath: Constraints on the polytropic index. *Geophysical Research Letters*, 18(10):1821–1824, 1991.

E. A. Helder, J. Vink, A. M. Bykov, Y. Ohira, J. C. Raymond, and R. Terrier. Observational Signatures of Particle Acceleration in Supernova Remnants. *Space Science Reviews*, 173(1):369–431, November 2012. ISSN 1572-9672. doi: 10.1007/s11214-012-9919-8.

A. Johlander, S. J. Schwartz, A. Vaivads, Yu. V. Khotyaintsev, I. Gingell, I. B. Peng, S. Markidis, P.-A. Lindqvist, R. E. Ergun, G. T. Marklund, F. Plaschke, W. Magnes, R. J. Strangeway, C. T. Russell, H. Wei, R. B. Torbert, W. R. Paterson, D. J. Gershman, J. C. Dorelli, L. A. Avanov, B. Lavraud, Y. Saito, B. L. Giles, C. J. Pollock, and J. L. Burch. Rippled quasiperpendicular shock observed by the magnetospheric multiscale spacecraft. *Phys. Rev. Lett.*, 117: 165101, Oct 2016. doi: 10.1103/PhysRevLett.117.165101.

J. R. Jokipii. The Heliospheric Termination Shock. *Space Science Reviews*, 176 (1):115–124, June 2013. ISSN 1572-9672. doi: 10.1007/s11214-012-9914-0.

J. H. King and N. E. Papitashvili. Solar wind spatial scales in and comparisons of hourly wind and ace plasma and magnetic field data. *Journal of Geophysical Research: Space Physics*, 110(A2), 2005. doi: https://doi.org/10.1029/2004JA010649.

V. Krasnoselskikh, B. Lembège, P. Savoini, and V. V. Lobzin. Nonstationarity of strong collisionless quasiperpendicular shocks: Theory and full particle numerical simulations. *Physics of Plasmas*, 9(4):1192–1209, April 2002. doi: 10.1063/1.1457465.

A. Lalti, Yu. V. Khotyaintsev, A. P. Dimmock, A. Johlander, D. B. Graham, and V. Olshevsky. A database of mms bow shock crossings compiled using machine learning. *Journal of Geophysical Research: Space Physics*, 127(8):e2022JA030454, 2022. doi: https://doi.org/10.1029/2022JA030454. e2022JA030454 2022JA030454.

B. Lembege and J. M. Dawson. Formation of double layers within an oblique collisionless shock. *Phys. Rev. Lett.*, 62:2683–2686, Jun 1989. doi: 10.1103/PhysRevLett.62.2683.

B Lembege and JM Dawson. Self-consistent study of a perpendicular collisionless and nonresistive shock. *The Physics of fluids*, 30(6):1767–1788, 1987.

O. Moullard, D. Burgess, T. S. Horbury, and E. A. Lucek. Ripples observed on the surface of the earth's quasi-perpendicular bow shock. *Journal of Geophysical Research: Space Physics*, 111(A9), 2006. doi: https://doi.org/10.1029/2005JA011594.

V. Olshevsky, Yu. V. Khotyaintsev, A. Lalti, A. Divin, G. L. Delzanno, S. Anderzén, P. Herman, S. W. D. Chien, L. Avanov, A. P. Dimmock, and S. Markidis. Automated classification of plasma regions using 3d particle energy distributions. *Journal of Geophysical Research: Space Physics*, 126(10):e2021JA029620, 2021. doi: https://doi.org/10.1029/2021JA029620. e2021JA029620 2021JA029620.

C. Pollock, T. Moore, A. Jacques, J. Burch, U. Gliese, Y. Saito, T. Omoto, L. Avanov, A. Barrie, V. Coffey, J. Dorelli, D. Gershman, B. Giles, T. Rosnack, C. Salo, S. Yokota, M. Adrian, C. Aoustin, C. Auletti, S. Aung, V. Bigio, N. Cao, M. Chandler, D. Chornay, K. Christian, G. Clark, G. Collinson, T. Corris, A. De Los Santos, R. Devlin, T. Diaz, T. Dickerson, C. Dickson, A. Diekmann, F. Diggs, C. Duncan, A. Figueroa-Vinas, C. Firman, M. Freeman, N. Galassi, K. Garcia, G. Goodhart, D. Guererro, J. Hageman, J. Hanley, E. Hemminger, M. Holland, M. Hutchins, T. James, W. Jones, S. Kreisler, J. Kujawski, V. Lavu, J. Lobell, E. LeCompte, A. Lukemire, E. MacDonald, A. Mariano, T. Mukai, K. Narayanan, Q. Nguyan, M. Onizuka, W. Paterson, S. Persyn, B. Piepgrass, F. Cheney, A. Rager, T. Raghuram, A. Ramil, L. Reichenthal, H. Rodriguez, J. Rouzaud, A. Rucker, Y. Saito, M. Samara, J.-A. Sauvaud, D. Schuster, M. Shappirio, K. Shelton, D. Sher, D. Smith, K. Smith, S. Smith, D. Steinfeld, R. Szymkiewicz, K. Tanimoto, J. Taylor, C. Tucker, K. Tull, A. Uhl, J. Vloet, P. Walpole, S. Weidner, D. White, G. Winkert, P.-S. Yeh, and M. Zeuch. Fast Plasma Investigation for Magnetospheric Multiscale. *Space Science Reviews*, 199(1):331–406, March 2016. ISSN 1572-9672. doi: 10.1007/s11214-016-0245-4.

C. T Russell. Planetary bow shocks. *Collisionless Shocks in the Heliosphere: Reviews of Current Research, Geophys. Monogr. Ser*, 35:109–130, 1985.

C. T. Russell, M. M. Hoppe, and W. A. Livesey. Overshoots in planetary bow shocks. *Nature*, 296(5852):45–48, March 1982. ISSN 1476-4687. doi: 10.1038/296045a0.

C. T. Russell, B. J. Anderson, W. Baumjohann, K. R. Bromund, D. Dearborn, D. Fischer, G. Le, H. K. Leinweber, D. Leneman, W. Magnes, J. D. Means, M. B. Moldwin, R. Nakamura, D. Pierce, F. Plaschke, K. M. Rowe, J. A. Slavin, R. J. Strangeway, R. Torbert, C. Hagen, I. Jernej, A. Valavanoglou, and I. Richter. The Magnetospheric Multiscale Magnetometers. *Space Science Reviews*, 199(1):189–256, March 2016. ISSN 1572-9672. doi: 10.1007/s11214-014-0057-3.

D. Winske and K. B. Quest. Magnetic field and density fluctuations at perpendicular supercritical collisionless shocks. *Journal of Geophysical Research: Space Physics*, 93(A9):9681–9693, 1988. doi: https://doi.org/10.1029/JA093iA09p09681.

Daniel Winterhalter and Margaret G. Kivelson. Observations of the earth's bow shock under high mach number/high plasma beta solar wind conditions. *Geophysical Research Letters*, 15(10):1161–1164, 1988. doi: https://doi.org/10.1029/GL015i010p01161.

Z. W Yang, Bertrand Lembège, and Q. M Lu. Impact of the rippling of a perpendicular shock front on ion dynamics. *Journal of Geophysical Research: Space Physics*, 117(A7), 2012.